Volume 1 | Number 1 | Jan 2013 | Pages 1–100

PCCP

Physical Chemistry Chemical Physics
www.rsc.org/pccp

ROYAL SOCIETY OF CHEMISTRY

ROYAL SOCIETY OF CHEMISTRY

www.rsc.org/pccp

Page 1 of 11

Physical Chemistry Chemical Physics
CREATED USING THE RSC LaTeX PCCP ARTICLE TEMPLATE – SEE www.rsc.org/electronicfiles FOR DETAILS

ARTICLE TYPE

www. rsc.org/xxxxxx | XXXXXXXX

Morphology and Charge Transport in Amorphous and Crystalline P3HT and PBTTT: Insights From Theory[†]

Domenico Alberga,[a] Aurélie Perrier,[b,c] Ilaria Ciofini,[b] Giuseppe Felice Mangiatordi,[d] Gianluca Lattanzi,[*a] and Carlo Adamo[*d,e]

We explore the connection between the morphology and the charge transport properties in Poly(3-hexylthiophene) (P3HT) and poly(2,5-bis(3-alkylthiophen-2-yl)thieno[3,2-b]thiophene) (PBTTT) semiconductor polymers in both amorphous and crystalline phases. Using Molecular Dynamics to simulate bulk supercells and the Marcus theory to analyze the transport properties we find that amorphous systems display a reduced hole mobility due to the loss of nematic order and $\pi - \pi$ stacking leading to a reduction in the electronic coupling between two chains. In crystal phase PBTTT displays a larger charge mobility than P3HT due to the interdigitation of the side chains enhancing the stability of the conjugated rings in the backbones. This more stable $\pi - \pi$ stacking reduces the energetic disorder with respect to P3HT and increases the electronic coupling. On the contrary, in the amorphous phase, PBTTT displays a reduced charge mobility with respect to P3HT caused by the absence of side chains attached to the thienothiophenes that increases their fluctuations and the energetic disorder. In addiction, we show that it is possible to calculate the reorganization energy neglecting the side chains of the polymers and thus saving computational time. Within this approximation, we obtain mobility values matching the experimental measures, thus confirming that the side chains are crucial to shape the morphology of the polymeric systems but are not involved in the charge transport process.

1 Introduction

Poly(3-hexylthiophene) (P3HT) and poly(2,5-bis(3-alkylthiophen-2-yl)thieno[3,2-b]thiophene) (PBTTT) (Fig.1) are two of the most studied semiconductor polymers having a wide range of applications ranging from organic thin-film transistors (OTFTs), solar cell, light emitting diodes to biosensors[1–6]. In particular they are successfully used as the organic semiconductor layer (OSL) in the OTFTs. The performances of OTFTs are typically evaluated in terms of mobility of charge carriers and are strongly affected by the morphology and the molecular order of the OSL[7]. P3HT and PBTTT display different characteristics that reflect into different device performances: OTFTs employing P3HT as semiconductor yielded a charge mobility value of 0.1-0.2 $cm^2V^{-1}s^{-1}$,[8] to be compared with 1.0 $cm^2V^{-1}s^{-1}$ in PBTTT devices[9]. Several experimental investigations were carried out to investigate the relevant differences between the morphology of P3HT and PBTTT thin films in order to explain the large difference found in the measured charge mobility. Atomic force microscope (AFM) images show that typically an OSL is polycrystalline with the alternation of crystalline domains separated by amorphous grain boundaries[7]. The latter form charge traps that hinder the charge carrier transport lowering the mobility. AFM images[7] show that PBTTT thin film own wider crystalline domains than P3HT. This is probably due to the lower density of the attached side chains in PBTTT that allows their interdigitation detected through X-ray spectroscopy studies[10]. Interdigitated polymeric chains generate stable conformations that favor the formation of large crystalline domains. On the contrary the interdigitation is absent in P3HT. This was confirmed by density functional theory (DFT) calculations[11,12] showing that the interdigitation is energetically favourable in PBTTT but not in P3HT. However, nuclear magnetic resonance (NMR) measurements[13] show that the absence of interdigitation in P3HT produce an increased side chain mobility that weakens the $\pi - \pi$ interactions between the thiophenes.

In this picture, computational techniques can help to understand the relation between the OSL morphology and the transport properties of charge carriers. In particular, in order to

[a] *Dipartimento di Fisica, Università di Bari "Aldo Moro", INFN & TIRES, Via Orabona 4, I-70126 Bari, Italy; E-mail: gianluca.lattanzi@uniba.it*
[b] *PSL Research University, Chimie ParisTech - CNRS, Institut de Recherche de Chimie Paris, F-75005, Paris, France; E-mail: carlo.adamo@chimie-paristech.fr*
[c] *Université Paris Diderot, Sorbonne Paris Cité, 5 rue Thomas Mann, 75205 Paris cedex 13, France.*
[d] *Dipartimento di Farmacia - Scienze del Farmaco, Università di Bari "Aldo Moro", Via Orabona, 4, I-70126 Bari, Italy.*
[e] *Institut Universitaire de France, 103 Bd Saint-Michel, F-75005 Paris, France.*
† Electronic Supplementary Information (ESI) available: details and parameters of the used force field. See DOI: 10.1039/b000000x/

obtain results directly comparable with the experimental measurements, techniques that are able to deal with large scale systems in reasonable computational time were recently developed. Among others, Molecular Dynamics (MD) has been proved to be particularly useful to obtain microscopic configurations of large systems. Such configurations can be, in a second step, used to calculate charge transport properties using different quantum methodologies. In particular, McMahon et al.[14], using the localized molecular orbital method (LMOM), demonstrated that in P3HT both the trap density and the density of states (DOS) shape are slightly affected by the presence of regioregularity defects. Mladenović and Vukmirović[15–17], using the Charge Patching Method (CPM) and the Overlapping Fragment Method (OFM), simulated a large scale model of P3HT demonstrating that the thermal disorder generates fluctuations in the long-range electrostatic potential causing the localization of charge carrier wave functions. Finally, Poelking et al.[18–20] using the Marcus Theory[21] showed the influence of polymorphism and temperature in the crystalline bulk of P3HT and PBTTT demonstrating that P3HT polymorph I displays a higher charge carrier mobility than the others polymorphs.

The computational methods used in these works try to obtain a realistic picture of the systems making a compromise between the size of the simulated polymeric model and the level of approximation used in the employed quantum method. All these works focus, in particular, on the description of P3HT and PBTTT properties in the crystal phase but an in depth comparison between the morphological and the charge transport properties of the two polymers in both crystalline and amorphous phases is still missing. Building on this context, the purpose of the present work is to study, trough MD simulations and Charge Transport Simulations based on the Marcus Theory[21], how the morphology and the order properties influence the charge transport in both crystalline and amorphous P3HT and PBTTT. First, we perform MD simulations on large scale models. The obtained configurations are analyzed through the calculation of several order parameters in order to describe the main morphological differences between the systems. Subsequently, we extract several configurations from the MD trajectories to calculate the charge carrier mobility. The obtained results allow to point out the link between the diversity of the morphology and the charge transport properties of the simulated systems.

2 Computational methods

2.1 MD computational strategy

Four systems were simulated: P3HT (Fig.1a) and PBTTT (Fig.1b) in both amorphous and crystalline phases. For the amorphous systems, MD trajectories from our previously pub-
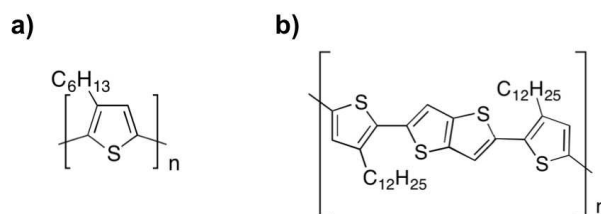

Fig. 1 Chemical structure of a) Poly(3-hexylthiophene) (P3HT) and b) poly(2,5-bis(3-alkylthiophen-2-yl)thieno[3,2-b]thiophene) (PBTTT) monomers.

lished work[22] where used. The latter were obtained simulating 60 P3HT regioregular chains of 18 monomers each and 48 PBTTT chains of 6 monomers each. The initial amorphous configurations were obtained starting from an ordered crystalline structure and running a first NPT simulation of 15 ns at a temperature of 800 K, which is well above the polymer melting point, and a pressure of 1 atm. The systems were gradually cooled down to the final temperature of 300 K in steps of 25 K every 200 ps. Following Do et al.[23], the time steps used were 1.6 fs for P3HT and 1.3 fs for PBTTT systems. The equilibrated simulation boxes were orthorhombic periodic boxes for both the amorphous P3HT and PBTTT with dimensions of $65.0 \times 103.0 \times 41.0$ Å^3 and $111 \times 56 \times 45$ Å^3 respectively. Representative snapshots of these two simulation boxes are reported in the ESI†. The total sampling time at the final temperature was 26 ns for P3HT and 23 ns for PBTTT.

For the crystalline systems 192 P3HT and PBTTT chains with the same number of monomer as before were simulated building a supercell starting from available crystallographic structures[24,25]. For P3HT we simulated the I polymorph that is proven to be the most thermodynamically stable[19] phase. Fig.2 reports the parameters of the primitive cell and representative snapshots of the periodic box showing the [010] and [001] crystallographic planes of the simulated system upon equilibration. The number of polymer chains in the three crystallographic directions were $N_a = 4$, $N_b = 16$ and $N_c = 3$ for both P3HT and PBTTT obtaining a monoclinic periodic box for P3HT (dimensions of $65.6 \times 62.2 \times 209.3$ Å^3; $\alpha = \beta = 90°$ $\gamma = 85.9°$) and a triclinic periodic box for PBTTT (dimensions of $78.7 \times 72.5 \times 331$ Å^3; $\alpha = 127°$ $\beta = 86°$ $\gamma = 90°$). After an equilibration run we sampled the NPT ensemble with a time step of 1.0 fs obtaining a 18 ns long trajectory for each system.

As in the previous work[22], the force fields for P3HT and PBTTT were parametrized following Do et al.[23] and Marcon and Raos[26]. All the details of the force field are reported in the ESI†. For the simulation of the four systems a cutoff was applied to van der Waals interactions at 12 Å using a switching function. All the MD simulations were performed using the NAMD 2.9 package[27]. In order to analyze and quantify the differences between the systems, a set of distribution functions
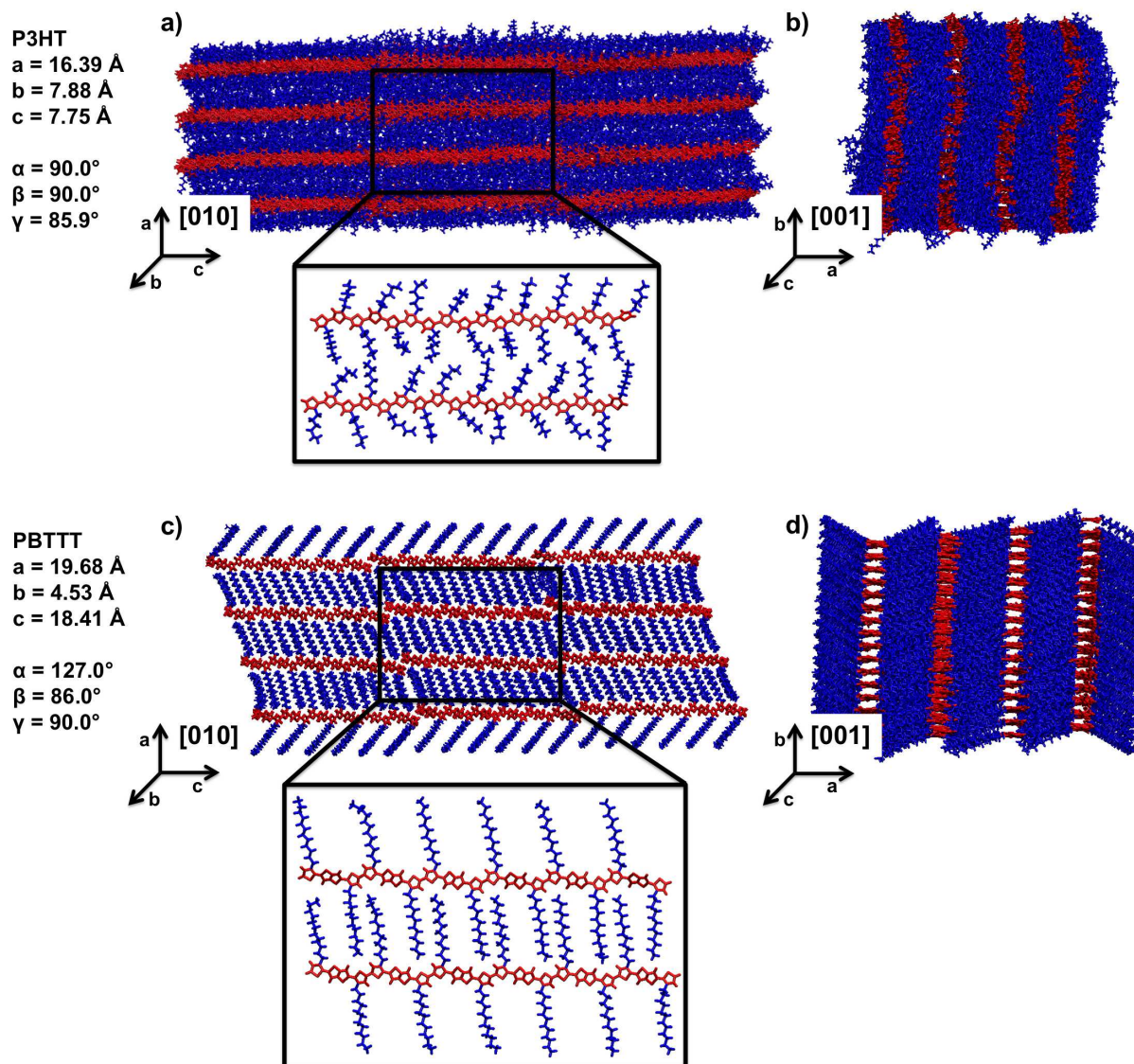
Fig. 2 Parameters of the primitive cell of P3HT and PBTTT and representative snapshots of the simulated crystalline systems upon equilibration: a) P3HT [010] plane, b) P3HT [001] plane, c) PBTTT [010] plane and d) PBTTT [001] plane. The backbones are depicted in red and the side chains in blue.

and order parameters were computed.

2.2 Charge Transport Simulations

In order to simulate charge transport in the four systems we used the nonadiabatic high-temperature limit of the semiclassical Marcus charge-transfer theory[21] based on the assumption that charges are localized on a single chain and charge transfer between two sites can be described by a hopping mechanism. In this framework, the hopping rate between two

molecules i and j can be computed as:

$$\omega_{ij} = \frac{J_{ij}^2}{\hbar} \sqrt{\frac{\pi}{\lambda_{ij} k_B T}} exp \left[-\frac{(\Delta E_{ij} - \lambda_{ij})^2}{4\lambda_{ij} k_B T} \right] \qquad (1)$$

where T is the temperature, J_{ij} the electronic coupling element between i and j, $\Delta E_{ij} = E_i - E_j$ the site energy difference, and λ_{ij}, the reorganization energy[21]. For all the calculations we considered only the polymer backbones replacing the side chains with hydrogen atoms. This approximation will be justified below. The electronic coupling elements are defined

as $J_{ij} = \langle \phi_i | \hat{H}_{ij} | \phi_j \rangle$ where $\hat{H}_{ij}$ is the dimer Hamiltonian and ϕ_i and ϕ_j are the highest occupied molecular orbitals extract from a DFT calculation performed on optimized structures using the B3LYP exchange and correlation functional and the 6-311G(d,p) basis set, as in ref. 18, for both P3HT and PBTTT backbones. J_{ij} values were calculated for each molecular pair ij from a neighbor list built with a cutoff of 12 Å, using the semiempirical ZINDO method[28,29]. E_i and E_j include the contributions of an external electric field $\vec{F}$ ($\Delta E_{ext} = -e\vec{F} \cdot \vec{d}_{ij}$ where $\vec{d}_{ij}$ is the vector joining the centers of mass of two backbones) and due to the Coulombic and polarization interactions between molecules within a given volume around the pair. These electrostatic interactions were calculated self-consistently using the Thole model[30,31], parametrized on the basis of the atomic polarizabilities and partial charges (generated via the Merz-Singh-Kollman scheme[32]) for a charged and a neutral molecule. The reorganization energy is the sum of two contributions: the intramolecular reorganization energy (λ_{in}) due to the relaxation of the nuclear degrees of freedom as the charge moves from donor i to acceptor j, and the intermolecular (outer sphere) reorganization energy (λ_{out}) due to the relaxation of the nuclear coordinates of the environment. In solids, such as the systems herein considered, $\lambda_{out} \approx 0.01$ eV because the geometries of the neighboring molecules do not change much during the charge transfer[18,19], and $\lambda \cong \lambda_{in}$ defined as

$$\lambda = E_{nC} - E_{nN} + E_{cN} - E_{cC} \qquad (2)$$

where E_{nN} (E_{cC}) is the energy of the neutral (charged) molecule in its optimized neutral (charged) geometry and E_{nC} (E_{cN}) is the energy of the neutral (charged) molecule in the optimized charged (neutral) geometry. These four terms were evaluated at the DFT level using the B3LYP functional and the 6-311G(d,p) basis set[18]. Charge-carrier dynamics was simulated by solving the master equation for a charge carrier drift-diffusion in an applied electric field using the calculated rates. All charge transport calculations were performed using the VOTCA package[33,34] and all DFT calculations with Gaussian09[35]. For the calculation we used 2000 frames extracted from the MD trajectories for each of the four simulated systems.

3   Results and discussion

3.1   MD simulations

Several order parameters were computed along the obtained MD trajectories to quantify the degree of order in the four simulated systems.

The nematic order parameter[18,19] (P_2) is defined in terms of

Table 1 Nematic order parameters for the simulated systems.

System	P_2 (TH)	P_2 (TT)
P3HT crystal	0.835 ± 0.006	
PBTTT crystal	0.959 ± 0.003	0.958 ± 0.003
P3HT amorphous	0.070 ± 0.001	
PBTTT amorphous	0.289 ± 0.008	0.256 ± 0.015

the unit vector $\hat{u}$ as the largest eigenvalue of the $Q_{\alpha\beta}$ tensor:

$$Q_{\alpha\beta} = \left\langle \frac{1}{N} \sum_{i=1}^{N} \left(\frac{3}{2} \hat{u}_{i\alpha} \hat{u}_{i\beta} - \frac{1}{2} \delta_{\alpha\beta} \right) \right\rangle \qquad (3)$$

where $\langle \ \rangle$ denotes a time average and N is the number of vectors involved in the average. A $P_2 = 1$ indicates a perfect nematic order with all unit vectors parallel to each other, while a value of $P_2 = 0$ corresponds to the total absence of order and describes a fully isotropic orientation. We calculated this parameter considering as $\hat{u}$ the unit vector normal to thiophene (TH) or thienothiophene (TT) rings. A high P_2 value would reveal the existence of a preferred ring orientation, given by the eigenvector corresponding to the P_2 eigenvalue. A high P_2 would also imply an improved $\pi - \pi$ stacking and hence a higher overlap of the π orbitals that would, consequently, lead to a higher charge carrier mobility and improved OTFT performances. The results obtained for the four systems analyzed are reported in Tab.1.

Obviously, crystalline systems have much higher P_2 values than the amorphous ones: in crystals we found an ordered repetition of the rings sharing the same orientation which instead becomes random in the amorphous phase. Nonetheless, it is worth noting that PBTTT has higher P_2 values than P3HT in both phases leading to an improved $\pi - \pi$ stacking that could explain the higher charge carrier mobility found in experiments[8,9].

The stability in time of the order described by the nematic order parameter is quantified by the dynamic order parameter[18,19] S defined as:

$$S = \left\langle \frac{1}{N} \sum_{i=1}^{N} \left(\frac{3}{2} \left(\hat{U}_i \cdot \hat{u}_i \right)^2 - \frac{1}{2} \right) \right\rangle \qquad (4)$$

where $\hat{U}_i = \langle \hat{u}_i \rangle$ and $\langle \ \rangle$ denotes a time average. Again, $\hat{u}$ was considered as the unit vector normal to thiophene (TH) or thienothiophene (TT) rings. S can range from 1 to -0.5: $S = 1$ implies a constant ring orientation, while a smaller S value indicates that the orientation is changing over time. The results obtained for the amorphous and crystalline systems analyzed are reported in Tab.2.

Again PBTTT presents higher S values than P3HT in both phases: in PBTTT the rings are characterized by less fluctuations in time than in P3HT, thus implying a more stable $\pi - \pi$
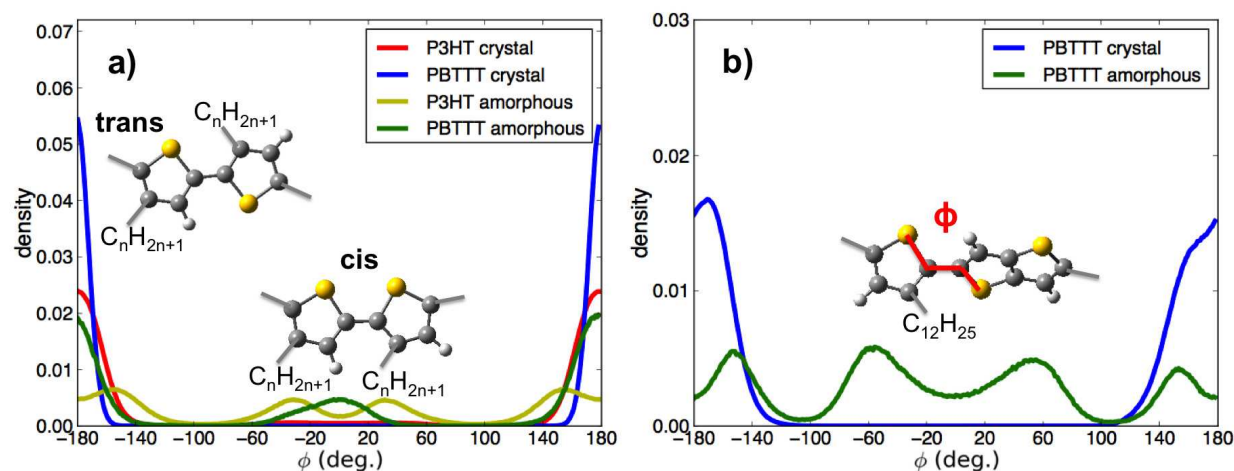
Fig. 3 Distribution of S-C-C-S dihedral angles between adjacent rings: a) TH-TH distributions, b) TH-TT distributions.
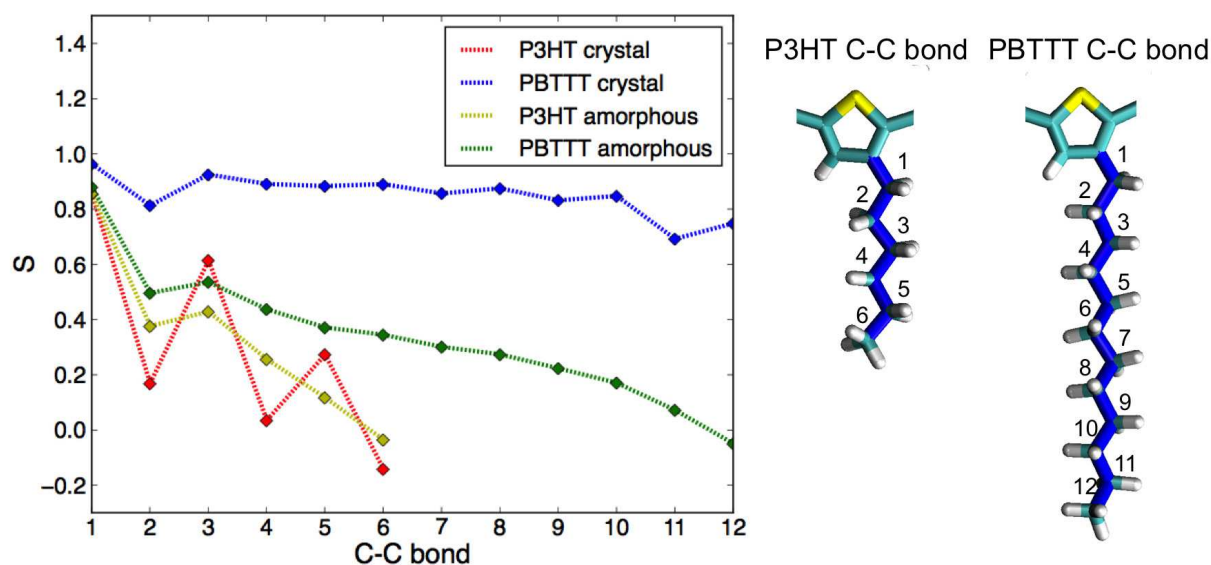

Fig. 4 Dynamic bond parameters of the carbon-carbon bond of the alkyl side chains (depicted in blue) for the simulated systems.

Table 2 Dynamic order parameters for the simulated systems.

System	S (TH)	S (TT)
P3HT crystal	0.846 ± 0.008	
PBTTT crystal	0.957 ± 0.001	0.947 ± 0.001
P3HT amorphous	0.828 ± 0.011	
PBTTT amorphous	0.870 ± 0.006	0.637 ± 0.011

stacking, due to the longer alkyl side chains of PBTTT that hinder the tilt of TH rings. In the amorphous phase, the fluctuations of the side chains weakens the order, thus allowing ring reorientation and leading to a reduction of S in both P3HT and PBTTT. Curiously, as far as the PBTTT amorphous state is concerned, a significant reduction of S can be detected in going from TH to TT, despite the absence of substantial differences in terms of P_2 (see Tab. 1). Although TT rings own an extra degree of freedom with respect to TH rings, due to the absence of a directly bounded side chain, the order and

stability in the crystal phase are ensured by the interdigitation of the side chains that hinders the rotation of TT rings. In the amorphous phase this interdigitation is lost thus reducing the steric hindrance around the TT rings that are now allowed to rotate with more freedom.

It is possible to further clarify this picture by plotting the distributions of the S-C-C-S dihedral angles (ϕ) defining the tilt angle between two adjacent TH-TH rings or TH-TT rings as reported in Fig.3.

ϕ values of 0 or 180° (-180°) describe situations where the adjacent rings are perfectly coplanar: in this situation the π orbitals are delocalized between the rings improving the inter-chain charge transport. Different ϕ values describe systems with a tilt between the two rings that decreases orbitals delo-calization and, thus, charge transport[36]. Moreover there is a difference between ϕ=0° and ϕ=180° in the TH-TH dihedral angle: a ϕ=180° describes a system where the side chains at-tached to the rings point in opposite directions (*trans* confor-mation), while if ϕ=0° the side chains are on the same side of the backbone (*cis* conformation) leading to a steric hin-drance that generates an unstable conformation[22,23]. In the crystal phase, TH-TH distributions display only a peak at 180° (-180°) for both P3HT and PBTTT. This peak is broader in P3HT than in PBTTT showing a greater ring fluctuation and deviation from the planar chain conformation, in agreement with the already discussed S values. Amorphous systems dis-play not only a broader distribution but also evidences of the presence of *cis* conformers. Furthermore, P3HT amorphous systems show a shift in the peaks to $\approx$ 30° and $\approx$ 150° show-ing a preferred deviation from the planarity that will eventu-ally result in a damage to intra-chain charge transport. This phenomenon is also evident in TH-TT dihedral angle distribu-tions of PBTTT systems (Fig.3b): in the crystal phase there is only one peak centered at 180° that splits in two possible peaks at (60° and 150°) in the amorphous phase. It is worth to notice that, in general, TH-TT dihedral angle distributions, in both crystal and amorphous phases of PBTTT, are broader than the corresponding TH-TH dihedral angle distributions. This is due to the absence of side chains that induces a greater conformational freedom for the TT rings in agreement with the reduced S values.

The stability of the side chains influences the stability of the orientation of the TH rings and could also be quantified by calculating the dynamic order parameter S (Eq. 4) taking $\hat{u}$ as the vector along the carbon-carbon bonds of the side chains. Fig.4 reports the values of S for all the bonds indexed starting from the one between the carbon atom of the ring and the first carbon atom of the alkyl chain depicted in blue.

For each system S values tend to decrease with increasing distance from the ring: away from the ring, the side chains experience a greater conformational freedom. All the S values of PBTTT are greater than those of P3HT because the side
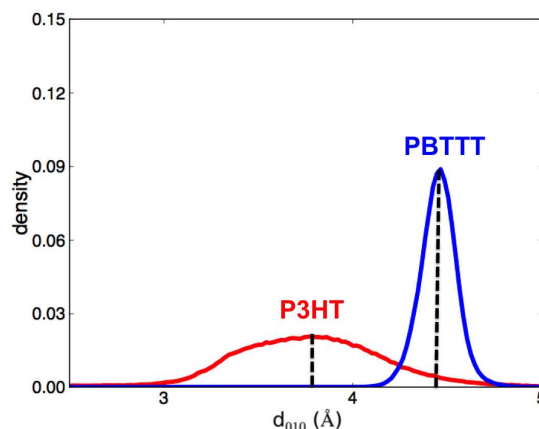

Fig. 5 Distribution of $\pi - \pi$ stacking distance d_{010} in crystal systems.

chains are stabilized by the interdigitation that reduce the mo-bility of the C-C bond even at large distances from the back-bone. This is evident by comparing Fig.2a and Fig.2c: the interdigitation of PBTTT side chains generates stable and or-dered conformations compared with those of P3HT that are more disordered due the absence of interdigitation. Interest-ingly, the S value does not substantially change in going from crystal to amorphous P3HT. On the contrary, in the amorphous phase of PBTTT, S values display an evident reduction spe-cially far from the backbone showing an increase in the mo-bility of the side chains. This phenomenon is probably due to the reduced side chain density of PBTTT with respect to that of P3HT[10], thus allowing the presence of increased free space in the PBTTT amorphous phase, that, in turn, allows an increased side chain mobility.

Finally the mobility of the side chains influences the fluc-tuations of the $\pi - \pi$ stacking distance in crystal phase, d_{010}, defined as the distance between the centers of mass of the two closest rings belonging to different polymer chains, projected on the 010-direction. The distribution of d_{010} is reported in Fig.5: although P3HT displays a smaller average $\pi - \pi$ stack-ing distance (3.77 Å) than PBTTT (4.46 Å), the corresponding distribution is much broader in P3HT. This is probably due to the greater mobility of the side chains that causes a high fluc-tuation in the distance between two adjacent polymers thus affecting charge transport. Notably, the average $\pi - \pi$ stack-ing distance in P3HT is comparable with the experimental value measured by combining X-ray diffraction and solid-state NMR[37] (3.90 Å), thus confirming the validity of our compu-tational model.

3.2 Charge Transport simulations

In this section we show how the conformational order described through MD simulations influence the charge transport properties of the four simulated systems. The calculated Marcus hopping rates were used to solve the master equation for a charge carrier drift-diffusion in an applied electric field and to calculate the hole mobility for these systems.

3.2.1 Calculation of the reorganization energy λ

3.2.1.1 Influence of the side chains. The calculation of the reorganization energy is the most demanding computational effort among the quantities in Eq.1. It requires two DFT geometry optimizations (neutral and charged molecule) whose convergence is affected by the number of degrees of freedom owned by the polymeric chains. In particular, the presence of the alkyl side chains represents the main issue to the convergence since the optimization algorithm has to explore the large conformational space often corresponding to geometric configurations with similar energy values and thus glowing the convergence. Here we demonstrate that it is possible to neglect the side chains in the calculation of λ replacing them with hydrogen atoms thus considering only the backbones of the polymers. Indeed under, this approximation, we obtained values of λ close to those obtained in the case of complete polymeric systems.

We have thus calculated λ for short model systems consisting of a chain of P3HT with 6 monomers and a chain of PBTTT with 2 monomers in four different ways: 1) optimization of polymer backbones (side chains replaced by H atoms) at the B3LYP/6-311G(d,p) level (λ_1); 2) optimization of full P3HT and PBTTT systems with ONIOM calculations[35] considering the backbones at the B3LYP/6-311G(d,p) level (high layer) and the side chains at the LDA/3-21G level (low layer) (λ_2); 3) using the full geometries obtained in 2) and calculating λ at the B3LYP/6-311G(d,p) level (λ_3); 4) using only the backbones geometries obtained in 2) (side chains replaced by H atoms) and calculating λ at the B3LYP/6-311G(d,p) level (λ_4). All these results are reported in Tab 3.

The difference among the calculated values is negligible in both P3HT and PBTTT. The comparison between λ calculated for the same optimized geometry with (λ_3) or without (λ_4) the side chains shows that the influence of their electronic structure has only a slight effect on λ (difference of 0.014 eV for P3HT and 0.002 eV for PBTTT). This is also confirmed by comparing λ calculated on the same geometry at the QM/QM' (λ_2) and at the full QM (λ_3) levels showing again a negligible influence of the electronic structure of the side chains (difference of 0.005 eV for P3HT and 0.001 eV for PBTTT). Finally, the comparison between λ calculated for the backbone optimized without (λ_1) or with the side chains (λ_4) displays that the impact of the structural modifications induced by the

Table 3 Calculation of the reorganization energy λ (eV) using four different strategies: 1) optimization of backbones at the B3LYP/6-311g(d,p) level (λ_1), 2) optimization of full P3HT and PBTTT with ONIOM calculations considering the backbones at the B3LYP/6-311g(d,p) level (high layer) and the side chains at the LDA/3-21g level (low layer) (λ_2), 3) using the full geometries obtained in 2) and calculating λ at the B3LYP/6-311g(d,p) level (λ_3), 4) using only the backbones geometries obtained in 2) and calculating λ at the B3LYP/6-311g(d,p) level (λ_4).

System	Model	λ
P3HT	λ_1	0.262
	λ_2	0.281
	λ_3	0.276
	λ_4	0.262
PBTTT	λ_1	0.241
	λ_2	0.261
	λ_3	0.260
	λ_4	0.258

presence of the side chains on the calculation of λ is trifling (differences below 0.001 eV for P3HT and of 0.017 eV for PBTTT). Moreover, in all these models we consistently find that $\lambda_{P3HT} > \lambda_{PBTTT}$, thus confirming the validity of our calculations. Taking into account these results we can assess that is possible to safely calculate the reorganization energy of these molecules excluding the side chains and thus saving computational time.

3.2.1.2 Influence of the number of monomers. We also investigated the dependence of λ on the number of monomers in P3HT and PBTTT chains. We calculated λ at the B3LYP/6-311G(d,p) level for P3HT backbones (model 1 in the previous paragraph) with 2, 4, 6, 12 and 18 monomers and for PBTTT backbones with 1, 2, 3, 4 and 6 monomers. Fig.6 shows the dependence of λ on the number of conjugated rings in the simulated systems (in PBTTT there are three rings for each monomer). It is clear that λ tends to converge with increasing number of rings: the number of monomers of the P3HT and PBTTT models used in our simulation (18 for P3HT and 6 for PBTTT) is a reasonable compromise in order to simulate a system with a λ resembling that of real polymeric chains with a greater number of monomers (more than 100) used in OTFT fabrication[1–6]. Again we always consistently find that $\lambda_{P3HT} > \lambda_{PBTTT}$.

3.2.1.3 Reorganization energy. For the longest polymers investigated within this study (P3HT with 18 monomers and PBTTT with 6 monomers) we have $\lambda_{P3HT} = 0.099$ eV and $\lambda_{PBTTT} = 0.085$ eV still using model 1. These values are very similar suggesting that the geometry relaxation that occurs during the charge hopping process is similar for the two poly-
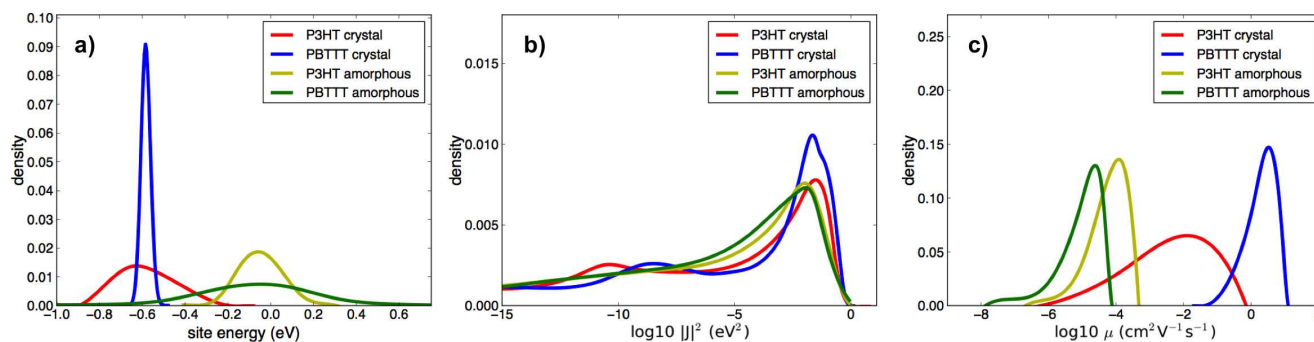
Fig. 7 Distributions of a) site energies, b) electronic coupling and c) hole mobility.
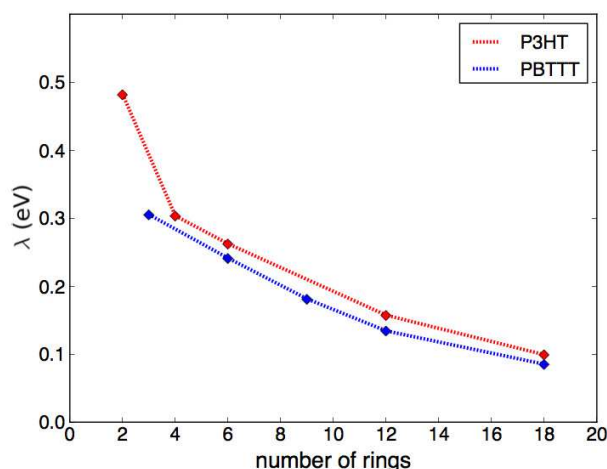

Fig. 6 Dependance of λ on the number of rings in P3HT and PBTTT backbones.

mers, thus the difference in the hole mobility experimentally found is caused essentially by the diversity in the morphology and order properties of the polymeric films, as described by the results of our MD study.

3.2.2 Site energy, electronic coupling and hole mobility
Fig.7a reports the distributions of the site energies, the differences between the energies of the system when the selected molecule is in its charged or neutral state excluding the constant internal contribution related to the gas-phase ionization potential. This quantity enters in the expression of Marcus charge hopping rates (Eq. 1) in the exponential as $\Delta E_{ij} = E_i - E_j$. Indeed the rates do not depend on a single energy value but on the energy differences between two sites. This implies that the distribution of ω_{ij} does not depend on the mean value of the site energies distribution but rather on its width also referred as energetic disorder[28]. A broad distri-

bution favors low ω_{ij} values while a peaked distribution generates high ω_{ij} thus improving the charge carrier mobility. Following the Gaussian Disorder Model,[38] it is possible to fit the site energy distribution with a Gaussian[39] function

$$f(E) = \frac{1}{\sqrt{2\pi}\sigma} exp\left[-\frac{1}{2}\left(\frac{E - \langle E \rangle}{\sigma}\right)^2\right] \quad (5)$$

where σ is the energetic disorder. In the crystal phase both PBTTT and P3HT distributions are centered around $\langle E \rangle \approx -0.58$ eV. However, PBTTT has a lower σ (22 meV) than P3HT (137 meV). The greater energetic disorder in P3HT is certainly related to the greater disorder already discussed and highlighted from MD results. In particular, the lower values of the nematic and dynamic order parameter imply a lower order and stability of P3HT chains, thus generating an energetic disorder that lowers the hole hopping rates hindering the overall charge carrier transport. On the contrary, PBTTT order properties lead to a low energetic disorder as pointed out by the narrow site energy distribution.

In the amorphous system the site energy distributions are centered around $\langle E \rangle \approx -0.08$ eV. In this case the energetic disorder is higher in PBTTT (363 meV) than in P3HT (103 meV). This is probably caused by the higher mobility of the TT rings as highlighted by the MD simulations (low S value and broad distribution of TH-TT dihedral angle).

Fig.7b shows the distributions of the electronic couplings for the four systems. A high electronic coupling leads to a high charge hopping rate. Crystal systems display a larger probability of high J_{ij} values than the amorphous ones: the presence of ordered and stable $\pi - \pi$ stacking typical of the crystal phase, described in the MD trajectories, favors the optimal overlap between orbitals enhancing the electronic couplings and charge transport. In the amorphous phase the low order and the poor presence of $\pi - \pi$ stacking generate low J_{ij} values. Moreover, the PBTTT crystal phase displays greater J_{ij} values than the P3HT crystal phase, in agreement with the

System	μ_{max}	μ_{exp}	Reference
P3HT crystal	10^{-2}	10^{-1}	8
PBTTT crystal	1	1	9
P3HT amorphous	10^{-4}	$< 10^{-3}$	40
PBTTT amorphous	10^{-5}	$< 10^{-3}$	40

Table 4 Order of magnitude of the most probable values of the charge carrier mobility μ_{max} $(cm^2V^{-1}s^{-1})$ for the four simulated systems calculated with an external electric field of 10^4 V/m applied in the $\pi - \pi$ stacking direction and experimental measurements μ_{exp} $(cm^2V^{-1}s^{-1})$.

higher nematic order reached by the PBTTT rings.

Finally, the charge hopping rates are used to solve the master equation for a charge carrier drift-diffusion in an applied electric field of 10^4 V/m in the transport direction (the $\pi - \pi$ stacking direction) and to calculate the charge carrier mobility. Fig.7c displays the distributions of the calculated mobilities for the four systems. The order of magnitude of the most probable values of the mobility (μ_{max}) are reported in Tab.4 along with the experimental measurements (μ_{exp}). The results are in agreement with the previously described site energy and electronic coupling distributions and with the order properties derived from the MD simulations: crystal phase systems display a greater μ_{max} than the amorphous ones due to the greater order. PBTTT in crystal phase shows a higher hole mobility than P3HT in crystal phase in line with the higher nematic and $\pi - \pi$ stacking order and stability. Finally, in amorphous phase PBTTT displays a lower hole mobility than P3HT due to the enhanced fluctuations of TT rings. As shown, these geometrical differences among the four systems are caused by the side chains of the polymers that strongly influence their properties of order and stability. The side chains do not directly take part in the charge transfer process, as demonstrated by the calculation of the reorganization energy, but strongly influence the morphology of the systems indirectly affecting the distributions of the site energies and the electronic couplings and thus the values of the hole mobility.

Finally, the results approximatively match the experimental measurements: in all cases except for P3HT in crystal phase μ_{max} is compatible with μ_{exp}. For P3HT in the crystal phase there is a difference of one order of magnitude in μ_{max} but the distribution of μ is broad and includes μ_{exp} with high probability. Note that μ_{exp} in the amorphous phase strongly depends on the fabrication conditions and the reported value of 10^{-3} $cm^2V^{-1}s^{-1}$ is the maximum value measured for these systems[40]. In this respect the calculated values are consistent with those provided by the experiments. These results confirm the reliability of the methods and approximations used.

4 Conclusions

We investigated how the differences in morphology and order among amorphous and crystalline P3HT and PBTTT affect the charge transport properties in these polymeric materials. Combining MD and charge transport simulations using the Marcus theory, we found that crystalline systems display a higher degree of nematic order than amorphous ones, thus influencing the $\pi - \pi$ stacking, the overlap between the orbitals of two adjacent polymeric chains and thus their electronic couplings. The reduction of the electronic couplings in amorphous systems leads to a low hole mobility. In crystal phase PBTTT displays a larger charge carrier mobility than P3HT: this is due to the greater stability of PBTTT backbones and side chains. The presence of the interdigitation of the side chains in PBTTT reduces their movements leading to reduced fluctuations of the conjugated rings and a sharper distribution of the dihedral angle between two consecutive rings and of the $\pi - \pi$ stacking distance. This generates a reduced energetic disorder and larger transport integrals resulting in a higher charge carrier mobility for PBTTT than for P3HT. Conversely, in the amorphous phase the absence of side chains attached to the thienothiophenes in PBTTT increases their fluctuations and the energetic disorder reducing the hole mobility.

The calculated mobilities are consistent with the experimental measurements confirming the validity of the models and approximations used. In particular, it is possible to neglect the side chains in the calculation of the reorganization energy without affecting the quality of the results and thus saving computational time. Moreover, this confirms that the side chains have a role only in shaping the morphological order of the systems but do not directly enter in the charge transfer process.

Acknowlegments

References

1 L. Torsi, N. Cioffi, C. D. Franco, L. Sabbatini, P. Zambonin and T. Bleve-Zacheo, *Solid-State Electron.*, 2001, **45**, 1479–1485.

2 M. D. Angione, M. Magliulo, S. Cotrone, A. Mallardi, D. Altamura, C. Giannini, N. Cioffi, L. Sabbatini, D. Gobeljic, G. Scamarcio, G. Palazzo and L. Torsi, *Biosens. Bioelectron.*, 2013, **40**, 303–307.

3 M. Magliulo, A. Mallardi, R. Gristina, F. Ridi, L. Sabbatini, N. Cioffi, G. Palazzo and L. Torsi, *Anal. Chem.*, 2013, **85**, 3849–3857.

4 K. Manoli, L. Dumitru, M. Mulla, M. Magliulo, C. Franco, M. Santacroce, G. Scamarcio and L. Torsi, *Sensors*, 2014, **14**, 16869–16880.

5 M. Magliulo, D. Altamura, C. D. Franco, M. V. Santacroce, K. Manoli,

A. Mallardi, G. Palazzo, G. Scamarcio, C. Giannini and L. Torsi, *J. Phys. Chem. C*, 2014, **118**, 15853–15862.

6 M. Y. Mulla, E. Tuccori, M. Magliulo, G. Lattanzi, G. Palazzo, K. Persaud and L. Torsi, *Nat. Comms.*, 2015, **6**, 6010.

7 I. McCulloch, M. Heeney, C. Bailey, K. Genevicius, I. MacDonald, M. Shkunov, D. Sparrowe, S. Tierney, R. Wagner, W. Zhang, M. L. Chabinyc, R. J. Kline, M. D. McGehee and M. F. Toney, *Nat. Mater.*, 2006, **5**, 328–333.

8 H. Sirringhaus, P. J. Brown, R. H. Friend, M. M. Nielsen, K. Bechgaard, B. M. W. Langeveld-Voss, A. J. H. Spiering, R. A. J. Janssen, E. W. Meijer, P. Herwig and D. M. de Leeuw, *Nature*, 1999, **401**, 685–688.

9 I. McCulloch, M. Heeney, M. L. Chabinyc, D. DeLongchamp, R. J. Kline, M. Cölle, W. Duffy, D. Fischer, D. Gundlach, B. Hamadani, R. Hamilton, L. Richter, A. Salleo, M. Shkunov, D. Sparrowe, S. Tierney and W. Zhang, *Adv. Mater.*, 2009, **21**, 1091–1109.

10 R. J. Kline, D. M. DeLongchamp, D. A. Fischer, E. K. Lin, L. J. Richter, M. L. Chabinyc, M. F. Toney, M. Heeney and I. McCulloch, *Macromolecules*, 2007, **40**, 7960–7965.

11 J. E. Northrup, *Phys. Rev. B*, 2007, **76**, 245202–245202–6.

12 R. Colle, G. Grosso, A. Ronzani and C. M. Zicovich Wilson, *Phys. Status Solidi B*, 2011, **248**, 1360–1368.

13 K. Yazawa, Y. Inoue, T. Shimizu, M. Tansho and N. Asakawa, *J. Phys. Chem. B*, 2010, **114**, 1241–1248.

14 D. P. McMahon, D. L. Cheung, L. Goris, J. Dacuña, A. Salleo and A. Troisi, *J. Phys. Chem. C*, 2011, **115**, 19386–19393.

15 N. Vukmirović and L.-W. Wang, *J. Phys. Chem. B*, 2009, **113**, 409–415.

16 N. Vukmirović and L.-W. Wang, *J. Phys. Chem. B*, 2011, **115**, 1792–1797.

17 M. Mladenović and N. Vukmirović, *Adv. Funct. Mat.*, 2014, n/a–n/a.

18 C. Poelking and D. Andrienko, *Macromolecules*, 2013, **46**, 8941–8956.

19 C. Poelking, E. Cho, A. Malafeev, V. Ivanov, K. Kremer, C. Risko, J.-L. Bredas and D. Andrienko, *J. Phys. Chem. C*, 2013, **117**, 1633–1640.

20 C. Poelking, K. Daoulas, A. Troisi and D. Andrienko, *Adv. Polym. Sci.*, 2014, 139–180.

21 R. Marcus, *Rev. Mod. Phys.*, 1993, **65**, 599–610.

22 D. Alberga, G. F. Mangiatordi, L. Torsi and G. Lattanzi, *J. Phys. Chem. C*, 2014, **118**, 8641–8655.

23 K. Do, D. M. Huang, R. Faller and A. J. Moule, *Phys. Chem. Chem. Phys.*, 2010, **12**, 14735–14739.

24 Z. Wu, A. Petzold, T. Henze, T. Thurn-Albrecht, R. H. Lohwasser, M. Sommer and M. Thelakkat, *Macromolecules*, 2010, **43**, 4646–4653.

25 E. Cho, C. Risko, D. Kim, R. Gysel, N. C. Miller, D. W. Breiby, M. D. McGehee, M. F. Toney, R. J. Kline and J.-L. Bredas, *J. Am. Chem. Soc.*, 2012, **134**, 6177–6190.

26 V. Marcon and G. Raos, *J. Am. Chem. Soc.*, 2006, **128**, 1408–1409.

27 J. C. Phillips, R. Braun, W. Wang, J. Gumbart, E. Tajkhorshid, E. Villa, C. Chipot, R. D. Skeel, L. Kale and K. Schulten, *J. Comput. Chem.*, 2005, **26**, 1781–1802.

28 V. Coropceanu, J. Cornil, D. A. da Silva Filho, Y. Olivier, R. Silbey and J.-L. Brédas, *Chem. Rev.*, 2007, **107**, 926–952.

29 J. Kirkpatrick, *Int. J. Quantum Chem.*, 2007, **108**, 51–56.

30 B. Thole, *Chem. Phys.*, 1981, **59**, 341–350.

31 P. T. van Duijnen and M. Swart, *J. Phys. Chem. A*, 1998, **102**, 2399–2407.

32 B. H. Besler, K. M. Merz and P. A. Kollman, *J. Comput. Chem.*, 1990, **11**, 431–439.

33 V. Rühle, C. Junghans, A. Lukyanov, K. Kremer and D. Andrienko, *J. Chem. Theory Comput.*, 2009, **5**, 3211–3223.

34 V. Rühle, A. Lukyanov, F. May, M. Schrader, T. Vehoff, J. Kirkpatrick, B. Baumeier and D. Andrienko, *J. Chem. Theory Comput.*, 2011, **7**, 3335–3345.

35 M. J. Frisch, G. W. Trucks, H. B. Schlegel, G. E. Scuseria, M. A. Robb, J. R. Cheeseman, G. Scalmani, V. Barone, B. Mennucci, G. A. Petersson, H. Nakatsuji, M. Caricato, X. Li, H. P. Hratchian, A. F. Izmaylov,

J. Bloino, G. Zheng, J. L. Sonnenberg, M. Hada, M. Ehara, K. Toyota, R. Fukuda, J. Hasegawa, M. Ishida, T. Nakajima, Y. Honda, O. Kitao, H. Nakai, T. Vreven, J. A. Montgomery, Jr., J. E. Peralta, F. Ogliaro, M. Bearpark, J. J. Heyd, E. Brothers, K. N. Kudin, V. N. Staroverov, R. Kobayashi, J. Normand, K. Raghavachari, A. Rendell, J. C. Burant, S. S. Iyengar, J. Tomasi, M. Cossi, N. Rega, J. M. Millam, M. Klene, J. E. Knox, J. B. Cross, V. Bakken, C. Adamo, J. Jaramillo, R. Gomperts, R. E. Stratmann, O. Yazyev, A. J. Austin, R. Cammi, C. Pomelli, J. W. Ochterski, R. L. Martin, K. Morokuma, V. G. Zakrzewski, G. A. Voth, P. Salvador, J. J. Dannenberg, S. Dapprich, A. D. Daniels, O. Farkas, J. B. Foresman, J. V. Ortiz, J. Cioslowski and D. J. Fox, *Gaussian09 Revision D.01*, Gaussian Inc. Wallingford CT 2009.

36 Y.-K. Lan, C. H. Yang and H.-C. Yang, *Polym. Int.*, 2010, **59**, 16–21.

37 D. Dudenko, A. Kiersnowski, J. Shu, W. Pisula, D. Sebastiani, H. W. Spiess and M. R. Hansen, *Angew. Chem. Int. Ed.*, 2012, **51**, 11068–11072.

38 H. Bässler, *Phys. Status Solidi B*, 1993, **175**, 15–56.

39 I. Yavuz, L. Zhang, A. L. Briseno and K. N. Houk, *J. Phys. Chem. C*, 2015, **119**, 158–165.

40 J. R. Reynolds and T. A. Skotheim, *Handbook of Conducting Polymers. Conjugated Polymers: Theory, Synthesis, Properties, and Characterization*, 2007.

Molecular Dynamics simulations and DFT calculations are combined via Marcus Theory to yield an estimate of charge carrier mobilities in the crystalline and amorphous phases of P3HT and PBTTT organic polymers.